BELLE-CONF-0109

Observation of Radiative B Meson Decays into Higher Kaonic Resonances

The Belle Collaboration

Abstract

We have studied radiative B meson decays into higher kaonic resonances decaying into a two-body or three-body final state, using a data sample of 21.3 fb^{-1} recorded at the $\Upsilon(4S)$ resonance with the Belle detector at KEKB. For the two-body final state, we extract the $B \to K_2^*(1430)\gamma$ component from an analysis of the helicity angle distribution, and obtain $\mathcal{B}(B^0 \to K_2^*(1430)^0\gamma) = (1.26 \pm 0.66 \pm 0.10) \times 10^{-5}$. For the three-body final state, we observe a $B \to K\pi\pi\gamma$ signal that is consistent with a mixture of $B \to K^*\pi\gamma$ and $B \to K\rho\gamma$. This is the first time that $B \to K^*\pi\gamma$ and $B \to K\rho\gamma$ have been observed separately. We find their branching fractions to be $\mathcal{B}(B \to K^*\pi\gamma; M_{K^*\pi} < 2.0\ \mathrm{GeV}/c^2) = (5.6 \pm 1.1 \pm 0.9) \times 10^{-5}$ and $\mathcal{B}(B \to K\rho\gamma; M_{K\rho} < 2.0\ \mathrm{GeV}/c^2) = (6.5 \pm 1.7\,^{+1.1}_{-1.2}) \times 10^{-5}$, respectively.

Typeset using REVTEX

K. Abe[9], K. Abe[37], R. Abe[27], I. Adachi[9], Byoung Sup Ahn[15], H. Aihara[39], M. Akatsu[20], K. Asai[21], M. Asai[10], Y. Asano[44], T. Aso[43], V. Aulchenko[2], T. Aushev[13], A. M. Bakich[35], E. Banas[25], S. Behari[9], P. K. Behera[45], D. Beiline[2], A. Bondar[2], A. Bozek[25], T. E. Browder[8], B. C. K. Casey[8], P. Chang[24], Y. Chao[24], K.-F. Chen[24], B. G. Cheon[34], R. Chistov[13], S.-K. Choi[7], Y. Choi[34], L. Y. Dong[12], J. Dragic[18], A. Drutskoy[13], S. Eidelman[2], V. Eiges[13], Y. Enari[20], C. W. Everton[18], F. Fang[8], H. Fujii[9], C. Fukunaga[41], M. Fukushima[11], A. Garmash[2,9], A. Gordon[18], K. Gotow[46], H. Guler[8], R. Guo[22], J. Haba[9], H. Hamasaki[9], K. Hanagaki[31], F. Handa[38], K. Hara[29], T. Hara[29], N. C. Hastings[18], H. Hayashii[21], M. Hazumi[29], E. M. Heenan[18], Y. Higasino[20], I. Higuchi[38], T. Higuchi[39], T. Hirai[40], H. Hirano[42], T. Hojo[29], T. Hokuue[20], Y. Hoshi[37], K. Hoshina[42], S. R. Hou[24], W.-S. Hou[24], S.-C. Hsu[24], H.-C. Huang[24], Y. Igarashi[9], T. Iijima[9], H. Ikeda[9], K. Ikeda[21], K. Inami[20], A. Ishikawa[20], H. Ishino[40], R. Itoh[9], G. Iwai[27], H. Iwasaki[9], Y. Iwasaki[9], D. J. Jackson[29], P. Jalocha[25], H. K. Jang[33], M. Jones[8], R. Kagan[13], H. Kakuno[40], J. Kaneko[40], J. H. Kang[48], J. S. Kang[15], P. Kapusta[25], N. Katayama[9], H. Kawai[3], H. Kawai[39], Y. Kawakami[20], N. Kawamura[1], T. Kawasaki[27], H. Kichimi[9], D. W. Kim[34], Heejong Kim[48], H. J. Kim[48], Hyunwoo Kim[15], S. K. Kim[33], T. H. Kim[48], K. Kinoshita[5], S. Kobayashi[32], S. Koishi[40], H. Konishi[42], K. Korotushenko[31], P. Krokovny[2], R. Kulasiri[5], S. Kumar[30], T. Kuniya[32], E. Kurihara[3], A. Kuzmin[2], Y.-J. Kwon[48], J. S. Lange[6], S. H. Lee[33], C. Leonidopoulos[31], Y.-S. Lin[24], D. Liventsev[13], R.-S. Lu[24], D. Marlow[31], T. Matsubara[39], S. Matsui[20], S. Matsumoto[4], T. Matsumoto[20], Y. Mikami[38], K. Misono[20], K. Miyabayashi[21], H. Miyake[29], H. Miyata[27], L. C. Moffitt[18], G. R. Moloney[18], G. F. Moorhead[18], N. Morgan[46], S. Mori[44], T. Mori[4], A. Murakami[32], T. Nagamine[38], Y. Nagasaka[10], Y. Nagashima[29], T. Nakadaira[39], T. Nakamura[40], E. Nakano[28], M. Nakao[9], H. Nakazawa[4], J. W. Nam[34], Z. Natkaniec[25], K. Neichi[37], S. Nishida[16], O. Nitoh[42], S. Noguchi[21], T. Nozaki[9], S. Ogawa[36], T. Ohshima[20], Y. Ohshima[40], T. Okabe[20], T. Okazaki[21], S. Okuno[14], S. L. Olsen[8], H. Ozaki[9], P. Pakhlov[13], H. Palka[25], C. S. Park[33], C. W. Park[15], H. Park[17], L. S. Peak[35], M. Peters[8], L. E. Piilonen[46], E. Prebys[31], J. L. Rodriguez[8], N. Root[2], M. Rozanska[25], K. Rybicki[25], J. Ryuko[29], H. Sagawa[9], Y. Sakai[9], H. Sakamoto[16], M. Satapathy[45], A. Satpathy[9,5], S. Schrenk[5], S. Semenov[13], K. Senyo[20], Y. Settai[4], M. E. Sevior[18], H. Shibuya[36], B. Shwartz[2], A. Sidorov[2], S. Stanič[44], A. Sugi[20], A. Sugiyama[20], K. Sumisawa[9], T. Sumiyoshi[9], J.-I. Suzuki[9], K. Suzuki[3], S. Suzuki[47], S. Y. Suzuki[9], S. K. Swain[8], H. Tajima[39], T. Takahashi[28], F. Takasaki[9], M. Takita[29], K. Tamai[9], N. Tamura[27], J. Tanaka[39], M. Tanaka[9], Y. Tanaka[19], G. N. Taylor[18], Y. Teramoto[28], M. Tomoto[9], T. Tomura[39], S. N. Tovey[18], K. Trabelsi[8], T. Tsuboyama[9], T. Tsukamoto[9], S. Uehara[9], K. Ueno[24], Y. Unno[3], S. Uno[9], Y. Ushiroda[9], S. E. Vahsen[31], K. E. Varvell[35], C. C. Wang[24], C. H. Wang[23], J. G. Wang[46], M.-Z. Wang[24], Y. Watanabe[40], E. Won[33], B. D. Yabsley[9], Y. Yamada[9], M. Yamaga[38], A. Yamaguchi[38], H. Yamamoto[8], T. Yamanaka[29], Y. Yamashita[26], M. Yamauchi[9], S. Yanaka[40], M. Yokoyama[39], K. Yoshida[20], Y. Yusa[38], H. Yuta[1], C. C. Zhang[12], J. Zhang[44], H. W. Zhao[9], Y. Zheng[8], V. Zhilich[2], and D. Žontar[44]

[1]Aomori University, Aomori
[2]Budker Institute of Nuclear Physics, Novosibirsk
[3]Chiba University, Chiba
[4]Chuo University, Tokyo
[5]University of Cincinnati, Cincinnati OH

[6]University of Frankfurt, Frankfurt
[7]Gyeongsang National University, Chinju
[8]University of Hawaii, Honolulu HI
[9]High Energy Accelerator Research Organization (KEK), Tsukuba
[10]Hiroshima Institute of Technology, Hiroshima
[11]Institute for Cosmic Ray Research, University of Tokyo, Tokyo
[12]Institute of High Energy Physics, Chinese Academy of Sciences, Beijing
[13]Institute for Theoretical and Experimental Physics, Moscow
[14]Kanagawa University, Yokohama
[15]Korea University, Seoul
[16]Kyoto University, Kyoto
[17]Kyungpook National University, Taegu
[18]University of Melbourne, Victoria
[19]Nagasaki Institute of Applied Science, Nagasaki
[20]Nagoya University, Nagoya
[21]Nara Women's University, Nara
[22]National Kaohsiung Normal University, Kaohsiung
[23]National Lien-Ho Institute of Technology, Miao Li
[24]National Taiwan University, Taipei
[25]H. Niewodniczanski Institute of Nuclear Physics, Krakow
[26]Nihon Dental College, Niigata
[27]Niigata University, Niigata
[28]Osaka City University, Osaka
[29]Osaka University, Osaka
[30]Panjab University, Chandigarh
[31]Princeton University, Princeton NJ
[32]Saga University, Saga
[33]Seoul National University, Seoul
[34]Sungkyunkwan University, Suwon
[35]University of Sydney, Sydney NSW
[36]Toho University, Funabashi
[37]Tohoku Gakuin University, Tagajo
[38]Tohoku University, Sendai
[39]University of Tokyo, Tokyo
[40]Tokyo Institute of Technology, Tokyo
[41]Tokyo Metropolitan University, Tokyo
[42]Tokyo University of Agriculture and Technology, Tokyo
[43]Toyama National College of Maritime Technology, Toyama
[44]University of Tsukuba, Tsukuba
[45]Utkal University, Bhubaneswer
[46]Virginia Polytechnic Institute and State University, Blacksburg VA
[47]Yokkaichi University, Yokkaichi
[48]Yonsei University, Seoul

I. INTRODUCTION

Radiative B meson decay through the $b \to s\gamma$ process has been one of the most sensitive probes of new physics beyond the Standard Model (SM). The inclusive picture of the $b \to s\gamma$ process is well established; however, our knowledge of the exclusive final states in radiative B meson decays is rather limited. To date, we know that around 15% of $b \to s\gamma$ can be accounted for by $B \to K^*(892)\gamma$ decays. In addition, a relativistic form-factor model calculation [1] predicts that another 20% of the $b \to s\gamma$ process should hadronize as one of the seven known higher kaonic resonances (Table I). CLEO has already reported an indication of the $B \to K_2^*(1430)\gamma$ signal [3]. Precision measurement of the inclusive $b \to s\gamma$ branching fraction will require detailed knowledge of such resonances, for example to model the decay processes into multi-particle final states. In this analysis, we study radiative B meson decay processes into higher kaonic resonances, which subsequently decay into two-body or three-body final states.

We have analyzed a data sample that contains 22.8×10^6 $B\bar{B}$ events. The data sample corresponds to an integrated luminosity of 21.3 fb^{-1} collected at the $\Upsilon(4S)$ resonance with the Belle detector [4] at the KEKB e^+e^- collider [5]. The beam energies are 3.5 GeV for positrons and 8 GeV for electrons.

Belle is a general purpose detector with a typical laboratory polar angular coverage between 17° to 150°. Charged tracks are reconstructed with a 50 layer central drift chamber (CDC), and are then extrapolated and refitted with a three layer double sided silicon vertex detector (SVD) to provide precision track information for the decay vertex reconstruction. Particle identification, namely discrimination of kaons from pions, is provided by combining information from silica aerogel Cherenkov counters (ACC) and a time-of-flight counter system (TOF), together with specific ionization (dE/dx) measurements from the CDC. Photons are measured with an electromagnetic calorimeter (ECL) of 8736 CsI(Tl) crystals. These detectors are surrounded by a 1.5 T superconducting solenoid coil.

TABLE I. Predicted branching fractions for radiative B decays into kaonic resonances.

	Theoretical prediction [$\times 10^{-5}$]		
mode	Veseli-Olsson [1]	Ali-Ohl-Mannel [2]	sub-decay modes
$B \to K^*(892)\gamma$	4.71 ± 1.79	1.4 − 4.9	$K\pi$ [∼100%]
$B \to K_1(1270)\gamma$	1.20 ± 0.44	1.8 − 4.0	$K\rho$ [42%], $K_0^*(1430)\pi$ [28%], $K^*(892)\pi$ [16%]
$B \to K_1(1400)\gamma$	0.58 ± 0.26	2.4 − 5.2	$K^*(892)\pi$ [94%], $K\rho$ [3%]
$B \to K^*(1410)\gamma$	1.14 ± 0.18	2.9 − 4.2	$K^*(892)\pi$ [>40%], $K\pi$ [6.6%]
$B \to K_2^*(1430)\gamma$	1.73 ± 0.80	6.9 − 14.8	$K\pi$ [49.9%], $K^*(892)\pi$ [24.7%]
$B \to K_2(1580)\gamma$	0.46 ± 0.11	1.8 − 2.6	$K^*(892)\pi$
$B \to K_1(1650)\gamma$	0.47 ± 0.16	(not given)	$K\pi\pi$, $K\phi$
$B \to K^*(1680)\gamma$	0.15 ± 0.04	0.4 − 0.6	$K\pi$ [38.7%], $K\rho$ [31.4%], $K^*(892)\pi$ [29.9%]

II. EVENT RECONSTRUCTION

We select events that contain a high energy (1.8 to 3.4 GeV in the $\Upsilon(4S)$ rest frame) photon (γ) candidate inside the acceptance of the barrel ECL ($33^\circ < \theta_\gamma < 128^\circ$). The photon candidate is required to be consistent with an isolated electromagnetic shower, i.e., 95% of its energy is concentrated in the central 3×3 crystals and there is no associated charged track. We combine it with other photon clusters in the event and reject it if the invariant mass of the pair is consistent with a π^0 or η.

Kaonic resonance (K_X) candidates are formed by combining one kaon with one or two pions, in the two-body $K^+\pi^-$, $K_S^0\pi^+$ and $K^+\pi^0$ final states and in the three-body $K^+\pi^-\pi^+$ final state. (Here and throughout the paper, charge conjugate modes are implicitly included.) For every charged particle track of good quality, the particle identification information is examined. A likelihood ratio for the kaon and pion probabilities is calculated by combining information from the ACC, TOF and dE/dx systems. We apply a tight cut with an efficiency of 85% for charged kaon candidates and a loose cut with an efficiency of 97% for charged pion candidates. Neutral pion (π^0) candidates are reconstructed from pairs of photons that satisfy the following requirements: the invariant two photon mass is consistent with a π^0, each photon has more than 50 MeV energy, the opening angle of two photons is less than 40° and one of the photons should deposit its energy in more than one crystal. The π^0 momentum is recalculated with a π^0 mass constraint. Neutral kaon ($K_S^0 \to \pi^+\pi^-$) candidates are reconstructed from two oppositely charged tracks, whose invariant mass is consistent with K_S^0. We require that the K_S^0 candidate form a vertex displaced from the interaction point and lie in a direction consistent with the K_S^0 momentum.

We reconstruct B meson candidates by forming two independent kinematic variables: the beam constrained mass and the energy difference. Both variables are calculated in the $\Upsilon(4S)$ rest frame. The beam constrained mass is defined as $M_{\rm bc} \equiv \sqrt{(E_{\rm beam})^2 - |\vec{p}_{K_X} + \vec{p}_\gamma|^2}$, in which the photon energy is constrained to be $E_\gamma = E_{\rm beam} - E_{K_X}$. This constraint improves the $M_{\rm bc}$ resolution by about 20%, resulting in an $M_{\rm bc}$ resolution of 3 MeV/c^2. The energy difference, $\Delta E \equiv E_{K_X} + E_\gamma - E_{\rm beam}$, has an asymmetric resolution, mainly due to energy leakage from the counters and energy loss in the inner material. We apply a cut of -100 MeV $< \Delta E <$ 75 MeV, which is about a 2σ cut on the higher side, and which removes around 25% of events on the lower side.

The largest background source is continuum light quark-pair ($q\bar{q}$) production, in which the high energy photon mainly comes from the initial state radiation ($e^+e^- \to q\bar{q}\gamma$) and decays of neutral hadrons ($\pi^0, \eta, \ldots$). In order to reduce such background, we form a Fisher discriminant which we call the *Super Fox-Wolfram* (SFW) variable [6],

$$SFW = \alpha_2 R_2^{\rm major} + \alpha_4 R_4^{\rm major} + \sum_{l=1}^{4} \beta_l R_l^{\rm minor},$$

$$R_l^{\rm major} = \frac{\sum_i |p_i||p_\gamma| P_l(\cos\theta_{i\gamma})}{\sum_i |p_i||p_\gamma|}, \quad R_l^{\rm minor} = \frac{\sum_{i,j} |p_i||p_j| P_l(\cos\theta_{ij})}{\sum_{i,j} |p_i||p_j|},$$

where l runs from 1 to 4 for the Legendre function P_l and i, j run over all the neutral and charged tracks that are not used to form the B candidate, and coefficients α_i and β_i are optimized to maximize the discrimination. The variable is calculated in the signal B

candidate rest frame rather than the $\Upsilon(4S)$ rest frame in order to eliminate any correlation with $M_{\rm bc}$. For further background suppression, we form a likelihood ratio (LR) from the SFW variable and the B meson flight direction ($\cos\theta_B$),

$$LR(SFW,\cos\theta_B) = \frac{p^{\rm sig}(SFW)p^{\rm sig}(\cos\theta_B)}{p^{\rm sig}(SFW)p^{\rm sig}(\cos\theta_B)+p^{\rm bg}(SFW)p^{\rm bg}(\cos\theta_B)},$$

where $p^{\rm sig}$ and $p^{\rm bg}$ are the probability density functions (PDF) for signal and background. The PDFs for the SFW are parametrized with an asymmetric Gaussian function. For $\cos\theta_B$, we use $p^{\rm sig}(\cos\theta_B) \propto \sin^2\theta_B$ for signal and a flat distribution for background. We require $LR > 0.7$ for the two-body K_X final states and $LR > 0.9$ for the three-body K_X final states. The LR cut efficiency is determined from the $B \to D\pi$ data samples using parametrizations determined from the signal and continuum $q\bar{q}$ Monte Carlo (MC) simulation samples.

The background from other B meson decays is examined with the corresponding MC samples. We find a negligible contribution from hadronic charmless decays. Background from $b \to c$ decays makes a non-negligible contribution in the sideband of negative ΔE especially at high K_X mass ($M_{K_X} > 1.5$ GeV/c^2), but does not contribute in the signal region. For the three-body final states, there is a small contribution from $B \to K^*(892)\gamma$ decays especially in the positive ΔE region; this contribution is removed by rejecting candidates if $M_{\rm bc}$ and ΔE calculated from $K^+\pi^-\gamma$ falls into the $K^*\gamma$ signal region. Cross-feed from other $b \to s\gamma$ final states is not negligible especially for the $K\pi\pi\gamma$ final state. These contributions are estimated using an inclusive $b \to s\gamma$ MC sample, and subtracted from the signal yield.

We extract the signal yield from a fit to the $M_{\rm bc}$ distribution. The shape is modeled as a sum of a Gaussian function for the signal and a threshold-type function (ARGUS function [7]) for the combinatoric background contribution. The normalizations are floated for both components. The signal function is fixed from the $B \to D\pi$ data. The background function is determined from ΔE sideband data in the range 0.1 GeV $< \Delta E <$ 0.5 GeV. Using a continuum $q\bar{q}$ MC sample, we check that the background shape has no visible correlation with ΔE. In order to estimate the systematic error of the fitting procedure, we vary the mean and width of the signal shape by $\pm 1\sigma$ and use the background shape from other sources, namely the continuum MC sample and the LR sideband ($LR < 0.3$) in which the signal contribution is negligible. We assign the largest deviation as the systematic error of the signal yield. As a cross-check, we fit the ΔE distribution with a signal shape from MC and a linear function for background with a slope determined from the $M_{\rm bc}$ sideband (5.2 GeV/$c^2 < M_{\rm bc} <$ 5.26 GeV/c^2), and obtain consistent results.

III. ANALYSIS OF $B \to K_2^*(1430)\gamma$

The $B \to K_2^*(1430)\gamma$ analysis is performed by requiring the $K\pi$ invariant mass to be within ± 125 MeV/c^2 of the nominal $K_2^*(1430)$ value. The results of fits to the $M_{\rm bc}$ distributions are shown in Fig. 1, separately for the neutral and charged modes. The signal yield is $29.1 \pm 6.7\,^{+2.4}_{-1.9}$ events for the neutral mode, of which the contribution from other $b \to s\gamma$ decays is estimated to be 0.4 ± 0.3 events; we also see some indication of a signal in the charged mode. These are consistent with the yields calculated from the ΔE distributions shown in Fig. 2.

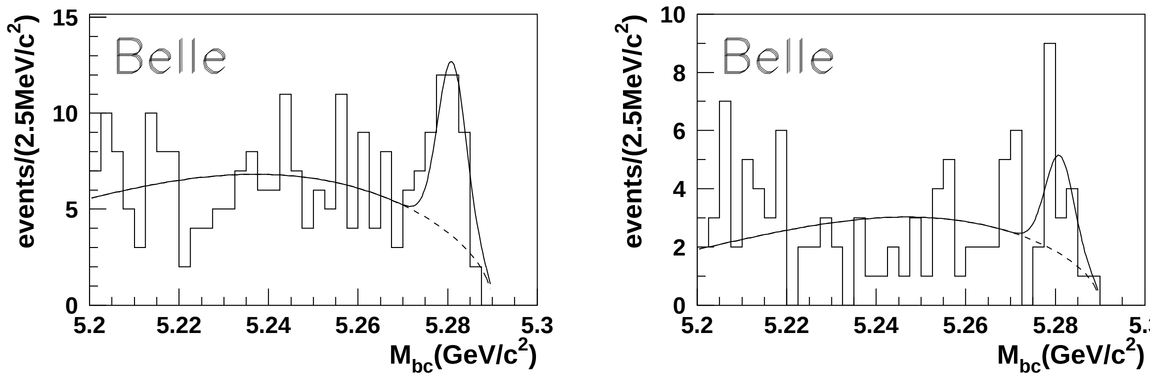

FIG. 1. The $M_{\rm bc}$ distributions for $B^0 \to K_2^*(1430)^0\gamma$ (left) and $B^+ \to K_2^*(1430)^+\gamma$ (right) candidates. The solid line is the fitting result. The background component is shown as the dashed line.

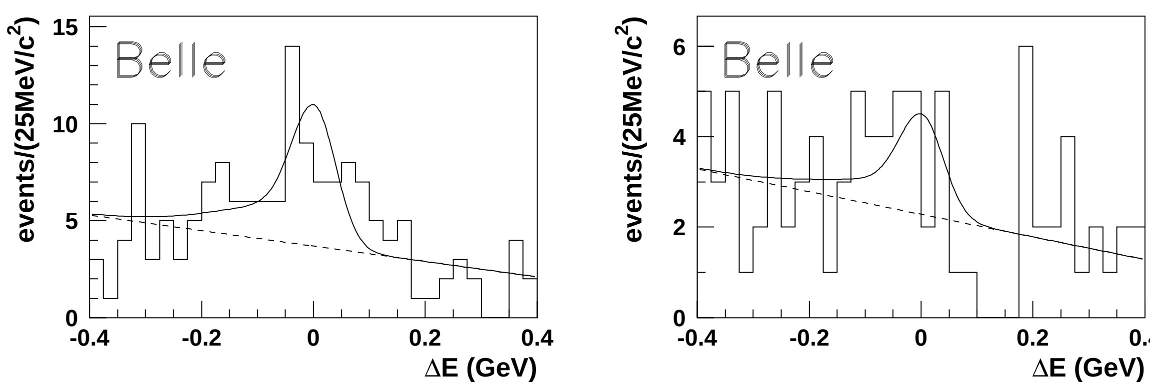

FIG. 2. The ΔE distributions for $B^0 \to K_2^*(1430)^0\gamma$ (left) and $B^+ \to K_2^*(1430)^+\gamma$ (right) candidates.

The event selection efficiency is determined from a MC sample that is calibrated with high statistics control data samples. Table II summarizes the sources of systematic error; a detailed description is given in Ref. [6]. The signal efficiency is $(6.99 \pm 0.55)\%$ for $B^0 \to K_2^*(1430)^0\gamma$, including the sub-decay branching fractions.

In order to distinguish the $B \to K_2^*(1430)\gamma$ signal from $B \to K^*(1410)\gamma$ and non-resonant decays, we examine the helicity angle distribution for the signal candidates. All three modes have different helicity distributions: $\cos^2\theta_{\rm hel} - \cos^4\theta_{\rm hel}$ for $K_2^*(1430)$, $1 - \cos^2\theta_{\rm hel}$ for $K^*(1410)$ and uniform for non-resonant decay. We divide $\cos\theta_{\rm hel}$ into 5 bins, and extract the yield from fits to the $M_{\rm bc}$ distribution for each bin (Fig. 3). This distribution clearly favors $B \to K_2^*(1430)\gamma$. We fit the $\cos\theta_{\rm hel}$ distribution with a function which is artificially parametrized to avoid a negative yield of $K^*(1410)$ or non-resonant component, and obtain 20.1 ± 10.5 events for the $B \to K_2^*(1430)\gamma$ component. After subtracting other $b \to s\gamma$ contributions, this leads to a $B^0 \to K_2^*(1430)^0\gamma$ branching fraction of

$$\mathcal{B}(B^0 \to K_2^*(1430)^0\gamma) = (1.26 \pm 0.66 \pm 0.10) \times 10^{-5}.$$

TABLE II. Contributions to the systematic error.

	$B \to K_2^*(1430)\gamma$	$B \to K\pi\pi\gamma$
photon reconstruction	5.3%	5.3%
charged track reconstruction	3.0%	4.4%
charged kaon selection	1.7%	1.7%
charged pion selection	0.6%	1.2%
L.R. + π^0/η veto + vertex	2.4%	5.1%
sub branching ratio uncertainty	2.4%	—
total	7.2%	9.1%

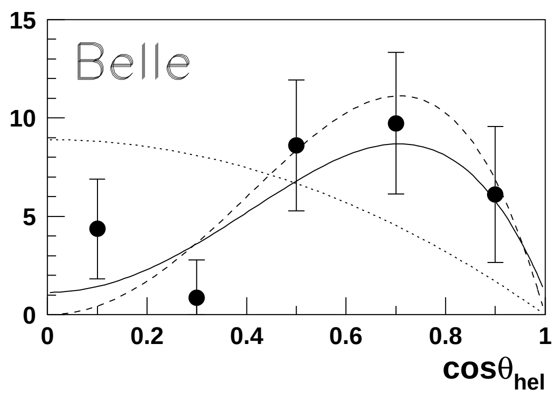

FIG. 3. The background subtracted $K_2^*(1430)$ helicity angle distribution. The solid curve is the fitting result. The theoretical curve for $B \to K_2^*(1430)\gamma$ ($B \to K^*(1410)\gamma$) is shown as the dashed (dotted) line.

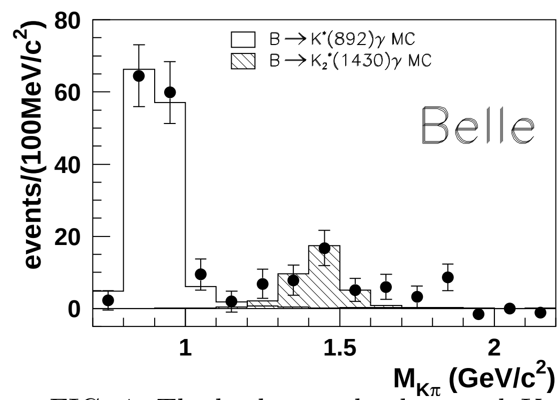

FIG. 4. The background subtracted $K\pi$ invariant mass distribution.

This result agrees with the prediction from the relativistic form-factor model of Veseli and Olsson [1], but is much lower than that from the non-relativistic form-factor model of Ali, Ohl and Mannel [2]. We also obtain the upper limit $\mathcal{B}(B^0 \to K^*(1410)^0\gamma) < 8.03 \times 10^{-5}$ (90% C.L.) by conservatively neglecting the non-resonant component in the fitting procedure.

The background subtracted $K\pi$ invariant mass distribution for $B \to K\pi\gamma$ is obtained by a similar method. We divide the $M_{K\pi}$ spectrum into 100 MeV/c^2 bins, and extract the signal yield from the $M_{\rm bc}$ distribution for each bin. In Fig. 4. we see a clear enhancement around 1.4 GeV/c^2, which supports the conclusion that the $B \to K_2^*(1430)\gamma$ contribution dominates.

IV. ANALYSIS OF $B \to K_X\gamma \to K\pi\pi\gamma$

The selection criteria used to reconstruct the $B \to K\pi\pi\gamma$ decay are identical to those used in the analysis of $B \to K_2^*(1430)\gamma$, unless explicitly stated otherwise. The K_X candidate is reconstructed from $K^+\pi^-\pi^+$, and required to have a mass between 1.0 GeV/c^2 and 2.0 GeV/c^2. The three charged tracks are required to form a vertex.

We select $B \to K_X\gamma \to K^*\pi\gamma$ candidates (here and throughout this section, K^* denotes $K^*(892)$ for simplicity) by requiring the invariant mass of $K^+\pi^-$ to be within ± 75 MeV/c^2 of the nominal K^* mass. The resulting $M_{\rm bc}$ and ΔE distributions are shown in Figs. 5 and 6, respectively. Using the same fitting procedure as is used for the $B \to K_2^*(1430)\gamma$ analysis, we obtain $46.4 \pm 7.3\,^{+1.6}_{-2.7}$ events from the $M_{\rm bc}$ distribution. This is consistent with the yield obtained from the ΔE distribution. These events are dominated by $B \to K^*\pi\gamma$ as a K^* mass peak is clearly seen in the $K\pi$ invariant mass distribution in Fig. 7. However, other contributions, which can arise either from $B^+ \to K^+\rho^0\gamma$ or non-resonant $B^+ \to K^+\pi^-\pi^+\gamma$, are not negligible. We estimate these contributions to be $5.8 \pm 2.2\,^{+0.3}_{-0.8}$ events from the region 1.1 GeV/$c^2 < M_{K\pi} <$ 1.4 GeV/c^2. An additional contribution from other $b \to s\gamma$ decay is estimated to be 0.9 ± 0.6 events from MC. After subtracting these non K^* contributions, we obtain a $B^+ \to K^{*0}\pi^+\gamma$ yield of $39.7 \pm 7.4\,^{+1.7}_{-2.6}$ events.

From the K_X invariant mass (M_{K_X}) distribution (Fig. 8), we observe a broad structure below 2.0 GeV/c^2 that can be explained, for example, as a sum of two known resonances around 1.4 GeV/c^2 and 1.7 GeV/c^2, but cannot be explained by a single known resonance or phase space decay. We observe no excess above 2.0 GeV/c^2, indicating that the $M_{K_X} <$ 2.0 GeV/c^2 cut does not introduce a significant inefficiency.

To estimate the efficiency of $B \to K^*\pi\gamma$, we analyze $B \to K_1(1400)\gamma$ and $B \to K^*(1680)\gamma$ MC samples, use the mean of the efficiencies as the central value, and assign the difference to the systematic error. As a result, the efficiency becomes $(3.13 \pm 0.47)\%$ including the other systematic errors in Table II. We determine the $B \to K^*\pi\gamma$ branching fraction,

$$\mathcal{B}(B \to K^*\pi\gamma; M_{K^*\pi} < 2.0~\text{GeV}/c^2) = (5.6 \pm 1.1 \pm 0.9) \times 10^{-5}.$$

There are four known resonances, $K_1(1270)$, $K_1(1400)$, $K^*(1410)$ and $K_2^*(1430)$, that can contribute to the signal around $M_{K_X} = 1.4$ GeV/c^2. In the region of 1.2 GeV/$c^2 < M_{K_X} <$ 1.6 GeV/c^2, we obtain $22.9 \pm 5.1\,^{+1.0}_{-1.7}$ events from the $M_{\rm bc}$ distribution. The $K_2^*(1430)$ contribution is estimated to be 2.6 ± 1.4 events from our branching fraction measurement, assuming $B^0 \to K_2^*(1430)^0\gamma$ and $B^+ \to K_2^*(1430)^+\gamma$ have equal branching fractions. The reconstruction efficiencies are about the same for $K_1(1400)\gamma$ and $K^*(1410)\gamma$ and a factor of two lower for $K_1(1270)\gamma$ including the $K_1(1270) \to K\rho$ and $K_1(1270) \to K_0^*(1430)\pi$ contributions. We interpret the signal yield as an upper limit on the weighted sum of the three resonances,

$$\frac{1}{2}\mathcal{B}(B \to K_1(1270)\gamma) + \mathcal{B}(B \to K_1(1400)\gamma) + \mathcal{B}(B \to K^*(1410)\gamma) \\ < 5.1 \times 10^{-5} \quad (90\%~\text{C.L.})$$

This limit on $\mathcal{B}(B \to K^*(1410)\gamma)$ is more stringent than that obtained from the $\cos\theta_{\rm hel}$ distribution of $K\pi\gamma$ decays.

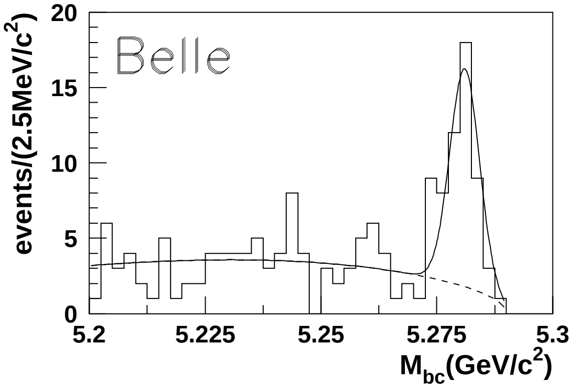

FIG. 5. The $M_{\rm bc}$ distribution for $B \to K^*\pi\gamma$ candidates.

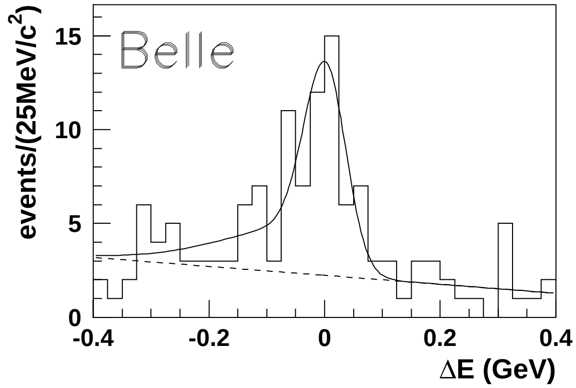

FIG. 6. The ΔE distribution for $B \to K^*\pi\gamma$ candidates.

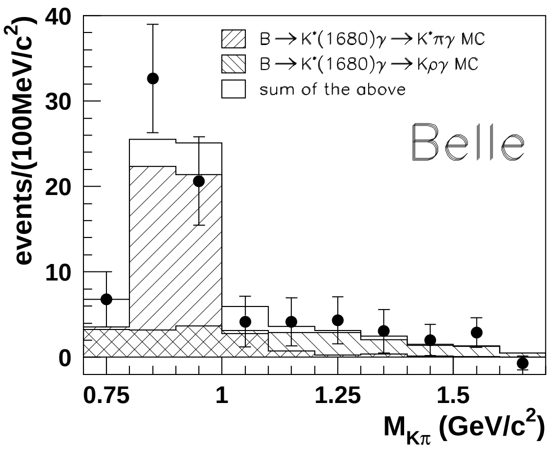

FIG. 7. The background subtracted K^* invariant mass distribution for the $B \to K^*\pi\gamma$ analysis.

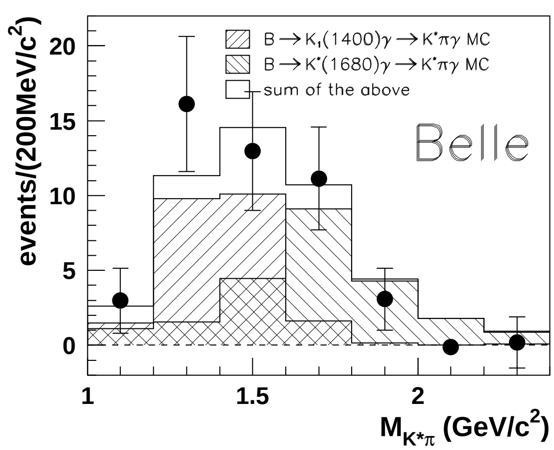

FIG. 8. The background subtracted $K\pi\pi$ invariant mass distribution for the $B \to K^*\pi\gamma$ analysis.

Next, we select $B \to K_X\gamma \to K\rho\gamma$ candidates by requiring the invariant mass of the $\pi^+\pi^-$ combination to be within ± 250 MeV/c^2 of the nominal ρ mass. To veto $B \to K_X\gamma \to K^*\pi\gamma$ events, we reject a candidate if the invariant $K^+\pi^-$ mass is within ± 125 MeV/c^2 of the nominal K^* mass. The $M_{\rm bc}$ distribution and the K_X invariant mass distribution are shown in Figs. 9 and 10, respectively. From the $M_{\rm bc}$ distribution, we obtain a signal yield of $24.5 \pm 6.4\,^{+1.2}_{-2.3}$ events. We subtract the contribution of 2.3 ± 1.2 events from other $b \to s\gamma$ decays.

The M_{K_X} spectrum of these events (Fig. 10) shows a large peak around 1.7 GeV/c^2. One possible explanation is a large $K^*(1680)\gamma$ component with a small contribution from $K_1(1270)$, but since there are quite a few resonances around 1.7 GeV/c^2, a detailed analysis will be required to disentangle the resonant substructure. The reconstruction efficiency for $B \to K\rho\gamma$, which is M_{K_X} dependent, is determined to be $(1.51 \pm 0.25)\%$ by assuming a

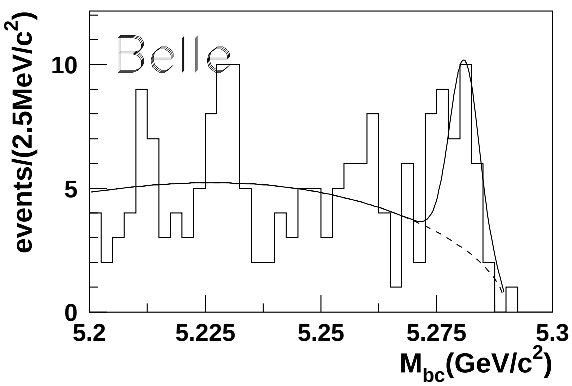

FIG. 9. The $M_{\rm bc}$ distribution for $B \to K\rho\gamma$ candidates.

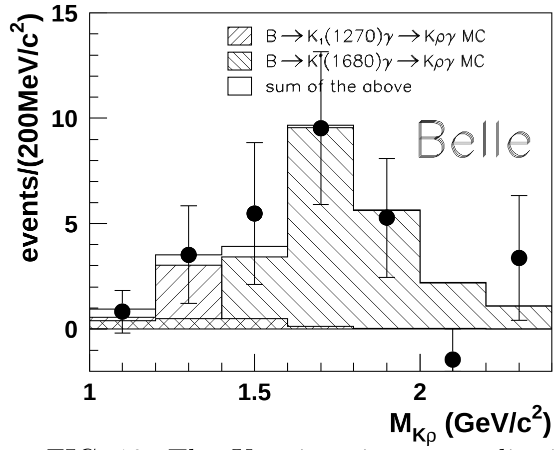

FIG. 10. The $K\pi\pi$ invariant mass distribution in the $B \to K\rho\gamma$ analysis. Background is subtracted in each bin.

mixture of $K_1(1270)$ and $K^*(1680)$ with a ratio from the M_{K_X} fit result. So far we find no signal outside the ρ mass window; neglecting the non-resonant $K\pi\pi\gamma$ contribution, we determine the $B \to K\rho\gamma$ branching fraction,

$$\mathcal{B}(B \to K\rho\gamma; M_{K\rho} < 2.0~\mathrm{GeV}/c^2) = (6.5 \pm 1.7\,^{+1.1}_{-1.2}) \times 10^{-5}.$$

The $K\rho\gamma$ final state in the mass range around 1.3 GeV/c^2 is effective for the search of $B \to K_1(1270)\gamma$, because the $K_1(1270)$ has a large ((42 $\pm$ 6)%) branching fraction to $K\rho$. The second largest contribution is from $K_2^*(1430) \to K\rho$ ((8.7 $\pm$ 0.8)%) from which we expect less than one event. Other contributions are much smaller. We search for $B \to K_1(1270)\gamma$ decays by requiring $|M_{K_X} - M_{K_1(1270)}| < 0.1$ GeV/c^2, as shown in Fig. 11. We find 4 candidates in the signal box with a background expectation of 1.19 events. Using a reconstruction efficiency of (0.41$\pm$0.06)%, we obtain an upper limit of $\mathcal{B}(B \to K_1(1270)\gamma) < 9.6 \times 10^{-5}$ (90% C.L.).

V. CONCLUSION

We have searched for radiative B meson decays into kaonic resonances that decay into a two-body or three-body final states together with a high energy photon. We observe sizable signals in $B \to K_2^*(1430)\gamma$, $B \to K^*\pi\gamma$ and $B \to K\rho\gamma$ decays and determine the branching fractions for these channels. The measured branching fractions respectively correspond to about 4%, 17% and 19% of the total $b \to s\gamma$ branching fraction assuming the SM calculation [9] or existing measurements [6,10,11] as the denominator. Adding 15% from the $K^*(892)\gamma$ branching fractions, these decay modes sum up to about half of the entire $b \to s\gamma$ process.

For the $K\pi\gamma$ final state, the $K_2^*(1430)\gamma$ component is separated from a possible $K^*(1410)\gamma$ or non-resonant contribution using a helicity angle analysis.

For the three-body final states, we observe $B \to K^*\pi\gamma$ and $B \to K\rho\gamma$ signals separately for the first time; however, the possible contribution of many kaonic resonances prevents

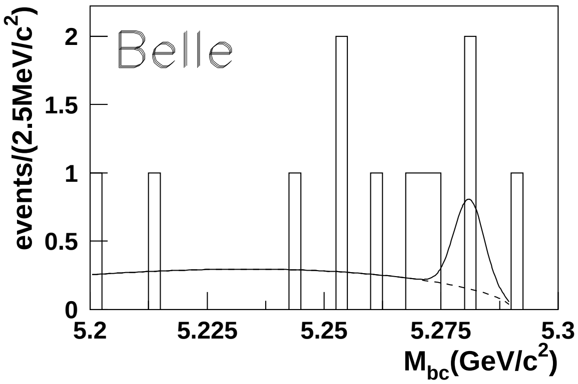

FIG. 11. The $M_{\rm bc}$ distribution for $B \to K_1(1270)\gamma$ candidates.

us from further identification of such resonances with the current statistics. We find no significant signal for $B \to K_1(1270)\gamma$ decay in the $K\rho\gamma$ final state.

VI. ACKNOWLEDGEMENT

We wish to thank the KEKB accelerator group for the excellent operation of the KEKB accelerator. We acknowledge support from the Ministry of Education, Culture, Sports, Science, and Technology of Japan and the Japan Society for the Promotion of Science; the Australian Research Council and the Australian Department of Industry, Science and Resources; the Department of Science and Technology of India; the BK21 program of the Ministry of Education of Korea and the CHEP SRC program of the Korea Science and Engineering Foundation; the Polish State Committee for Scientific Research under contract No.2P03B 17017; the Ministry of Science and Technology of Russian Federation; the National Science Council and the Ministry of Education of Taiwan; the Japan-Taiwan Cooperative Program of the Interchange Association; and the U.S. Department of Energy.

REFERENCES

[1] S.Veseli and M.G.Olsson, Phys. Lett. B **367**, 309 (1996).

[2] A.Ali, T.Ohl and T.Mannel, Phys. Lett. B **298**, 195 (1993)

[3] CLEO Collaboration, T.E.Coan *et al.*, Phys. Rev. Let. **84**, 5283 (2000).

[4] Belle Collaboration, K. Abe *et al.*, KEK Progress Report 2000-4 (2000), to be published in Nucl. Inst. and Meth. A.

[5] KEKB B Factory Design Report, KEK Report 95-7 (1995), unpublished; Y. Funakoshi *et al.*, Proc. 2000 European Particle Accelerator Conference, Vienna (2000).

[6] Belle Collaboration, K.Abe *et al.*, Phys. Lett. B **511**, 151 (2001).

[7] ARGUS Collaboration, H. Albrecht *et al.*, Phys. Lett. B **241**, 278 (1990).

[8] Particle Data Group, D.E. Groom *et al.*, Eur. Phys. J. **C15**, 1 (2000).

[9] K.Chetyrkin, M.Misiak, M.Münz, Phys. Lett. B **400**, 206 (1997); Erratum ibid. B **425**, 414 (1998)

[10] CLEO Collaboration, M.Alam *et al.*, Phys. Rev. Lett. **74**, 2885 (1995).

[11] ALEPH Collaboration, R.Barate *et al.*, Phys. Lett. B **429**, 196 (1998)